A1152D mutation of the Na^+ channel causes paramyotonia congenita and emphasizes the role of DIII/S4–S5 linker in fast inactivation

Magali Bouhours[1,2], Sandrine Luce[1], Damien Sternberg[3], Jean Claude Willer[2], Bertrand Fontaine[1] and Nacira Tabti[1,2]

[1]*INSERM U546 and* [2]*Laboratoire de Neurophysiologie, Faculté de Médecine Pitié-Salpêtrière, UPMC, 75013 Paris, France*
[3]*Laboratoire de Biochimie, Groupe Hospitalier Pitié-Salpêtrière, 75013 Paris, France*

Missense mutations in the human skeletal muscle Na^+ channel α subunit (hSkM1) are responsible for a number of muscle excitability disorders. Among them, paramyotonia congenita (PC) is characterized by episodes of muscle stiffness induced by cold and aggravated by exercise. We have identified a new PC-associated mutation, which substitutes aspartic acid for a conserved alanine in the S4–S5 linker of domain III (A1152D). This residue is of particular interest since its homologue in the rat brain type II Na^+ channel has been suggested as an essential receptor site for the fast inactivation particle. To identify the biophysical changes induced by the A1152D mutation, we stably expressed hSkM1 mutant or wild-type (WT) channels in HEK293 (human embryonic kidney) cells, and recorded whole-cell Na^+ currents with the patch-clamp technique. Experiments were performed both at 21 and 11°C to better understand the sensitivity to cold of paramyotonia. The A1152D mutation disrupted channel fast inactivation. In comparison to the WT, mutant channels inactivated with slower kinetics and displayed a 5 mV depolarizing shift in the voltage dependence of the steady-state. The other noticeable defect of A1152D mutant channels was an accelerated rate of deactivation from the inactivated state. Decreasing temperature by 10°C amplified the differences in channel gating kinetics between mutant and WT, and unveiled differences in both the sustained current and channel deactivation from the open state. Overall, cold-exacerbated mutant defects may result in a sufficient excess of Na^+ influx to produce repetitive firing and myotonia. In the light of previous reports, our data point to functional as well as phenotypic differences between mutations of conserved S4–S5 residues in domains II and III of the human skeletal muscle Na^+ channel.

(Received 10 December 2004; accepted after revision 22 March 2005; first published online 24 March 2005)
Corresponding author N. Tabti: INSERM U546, Laboratoire de Neurophysiologie, Faculté de Médecine Pitié-Salpêtrière, 91 Bd de l'Hôpital, 75013 Paris, France. Email: nacira.tabti@chups.jussieu.fr

Excitability of the skeletal muscle depends on the opening of voltage-gated Na^+ channels in response to membrane depolarization initiated physiologically by the end plate potential. Activation of the Na^+ channels is essential for the upstroke of the action potential, and their subsequent inactivation contributes to membrane repolarization (Hille, 1982). In the last decade, inherited muscle excitability disorders known as periodic paralyses (PP), paramyotonia congenita (PC) and potassium-aggravated myotonia (PAM) have been linked to the skeletal muscle Na^+ channel (Fontaine *et al.* 1990; McClatchey *et al.* 1992*a*; Ptacek, 1998). Genetic screening by different groups has disclosed at least 30 allelic missense mutations of the *SCN4A* gene encoding the pore forming α subunit (hSkM1) of the Na^+ channel (Cannon, 2000; Lehmann-Horn *et al.* 2002). Disease-causing hSkM1 mutations can be found in all four domains with a predilection for the intracellular regions. PC is characterized by cold-sensitive muscle stiffness that can be worsened by exercise. Patients with PC may also occasionally suffer from episodes of muscle weakness (Ptacek *et al.* 1992; Plassart *et al.* 1996). The electromyographic expression of myotonia is unmistakable, and consists of an outburst of high-frequency action potentials (myotonic discharges) on insertion of the needle electrode into the patient's muscles, or following single motor nerve stimulation (Fournier *et al.* 2004). The molecular basis of muscle hyper-excitability in PC has been investigated using heterologous systems to express mutant channels and identify their biophysical defects (McClatchey *et al.* 1992*b*; Cannon &

 DOI: 10.1113/jphysiol.2004.081018

Strittmatter, 1993; Cummins *et al.* 1993). One of the most common alterations induced by PC mutations is an impairment of Na^+ channel fast inactivation mainly seen as a reduced rate of inactivation and a depolarizing shift in the voltage dependence (Chahine *et al.* 1994; Yang *et al.* 1994; Hayward *et al.* 1996). Although such changes may account for membrane hyperexcitability through prolonged Na^+ influx, impairment of fast inactivation is not the unique determinant of paramyotonia. More recent studies have pointed out other gating defects such as slowed channel deactivation (Featherstone *et al.* 1998; Groome *et al.* 1999), or subtle changes in channel slow inactivation that may explain phenotypic variation between different PC mutations (Bouhours *et al.* 2004). The biophysical mechanisms underlying the sensitivity to cold of paramyotonia have not been systematically studied and need further clarification. Lowering the temperature is known to slow down Na^+ channel gating and induce some subtle shifts in the voltage dependence of fast and slow inactivation (Ruff, 1999). In PC mutants, slowing of fast inactivation and deactivation kinetics is exacerbated by cold. However, in most cases, this did not imply higher temperature sensitivity of mutant channels as compared to the wild-type (WT) (Yang *et al.* 1994; Fleischhauer *et al.* 1998; Mohammadi *et al.* 2003; Bouhours *et al.* 2004). The most prevalent mutations associated with PC are located in the DIII–DIV linker (T1313) and in the DIV/S4 segment (R1448) (Ptacek, 1998; Cannon, 2000). Other regions have also been sporadically implicated (Koch *et al.* 1995; Ji *et al.* 1996). We have identified a new mutation in the DIII/S4–S5 linker that substitutes a negatively charged residue for a hydrophobic one at position 1152 (A1152D). This mutation lies near the middle of the S4–S5 loop, a few residues upstream from two other mutations, the A1156T and I1160V, causing distinct clinical phenotypes (PC/hyperkalaemic periodic paralysis and PAM, respectively) (Ptacek *et al.* 1994; Yang *et al.* 1994; Richmond *et al.* 1997). S4–S5 loops in domains III and IV have been shown to play an important role in channel fast inactivation (Mitrovic *et al.* 1996; Tang *et al.* 1996; Lerche *et al.* 1997; Filatov *et al.* 1998), presumably by forming a docking site for the DIII–DIV inactivation particle (Smith & Goldin, 1997; McPhee *et al.* 1998; Miyamoto *et al.* 2001). Recently, a cooperative effect of DIII/and DIV/S4–S5 loops on fast inactivation has also been suggested (Popa *et al.* 2004). We studied the effects of the A1152D mutation both to get more insight into the pathophysiology of PC, and to better understand the role of the A1152 residue in Na^+ channel function. We expressed A1152D mutant channels in human embryonic kidney cells (HEK), and carried out a detailed biophysical analysis of the whole-cell Na^+ current. Experiments were also performed at 11°C to disclose the biophysical basis of the cold sensitivity of PC. Our results show that the A1152D mutation mainly impairs channel fast inactivation, has a slight effect on the kinetics of deactivation, and modifies neither the voltage dependence nor the onset of slow inactivation. These data point again to the pathogenic role of fast inactivation in PC. They also confirm the prominent role of the central alanine residue of DIII/S4–S5 in channel fast inactivation, presumably through its interaction with hydrophobic residues of the DIII–DIV fast inactivation particle (Tang *et al.* 1996; Smith & Goldin, 1997). Relative changes of gating kinetics with cold were more pronounced for the A1152D channel than for the WT, suggesting a higher temperature sensitivity for the mutant. Nevertheless, as observed for other PC mutants, A1152D fast inactivation time constants were further enhanced with cooling, thereby reaching levels that may represent the threshold for cold-induced myotonia.

Methods

Evaluation of patients

Clinical studies and sampling of family members were subject to a prior informed consent in accordance with French rules and the Helsinki convention. The index-case patient, a 74-year-old women of Caucasian origin, had suffered from cold-induced muscle stiffness since the age of five. She mainly complained of stiffness in the arms and legs, and had great difficulties in quickly opening her eyes under all circumstances. She did not report any episode of paralysis. One of her daughters had a similar clinical history; other members of the family were not affected (see pedigree structure in Fig. 1*A*). Clinical examination of the index patient disclosed spontaneous myotonia of the hand and the eyelids. In addition, typical myotonic discharges were readily detected in resting muscles using electromyography.

Genetic analysis

Genomic DNA was extracted from blood samples either by the classical phenol–chloroform protocol or by a rapid procedure using Quiagen DNA Minikit. The search for nucleotide alterations in PC patient DNA was performed by polymerase chain reaction (PCR) amplification of all 24 exons of the *SCNA4* gene, and single-strand conformation analysis of the amplified products (PCR–SSCA) (Jurkat-Rott *et al.* 2000). Samples demonstrating a shift of SSCA mobility were entirely sequenced using an automated sequencer (ABI PRISM 310, Applied Biosystems, CA, USA).

Site-directed mutagenesis

Site-directed mutagenesis of the human WT *SCN4A* cDNA in pRc/CMV vector (George *et al.* 1992) was performed using the Quickchange kit (Stratagene, La Jolla, CA, USA). Synthetic oligo-nucleotide primers containing

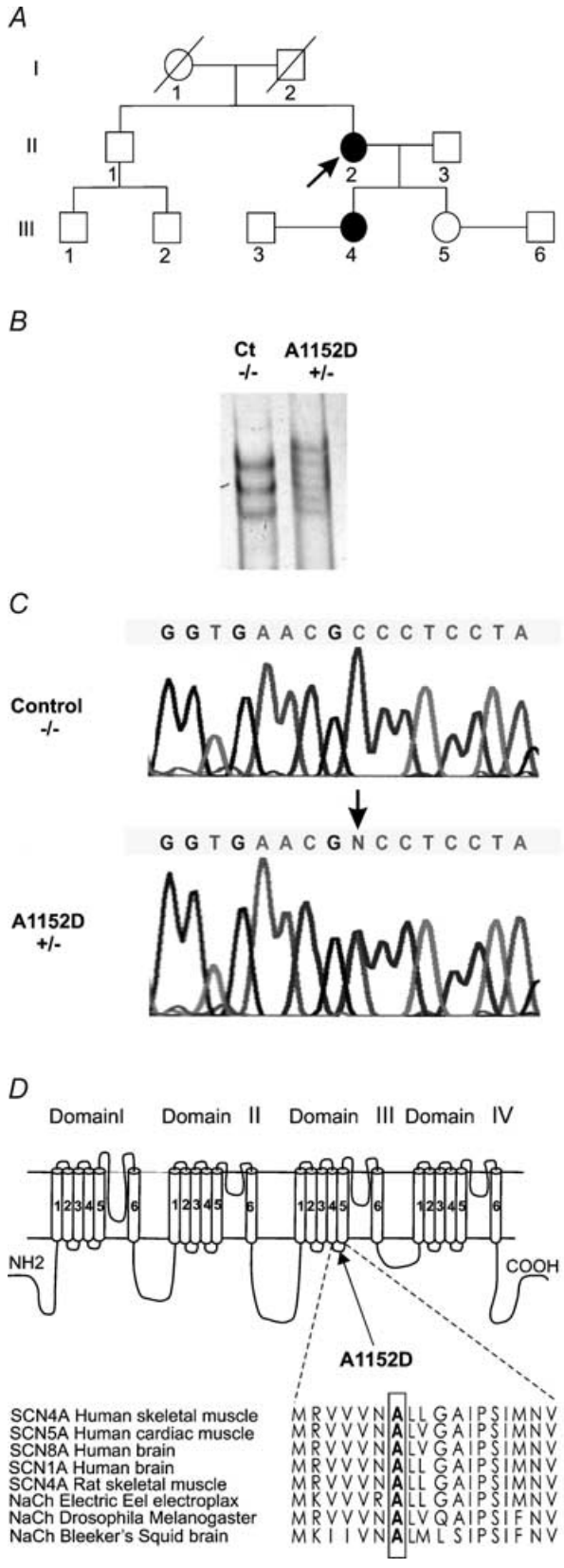

Figure 1. Genetic evidence of A1152D mutation
A, pedigree structure of the A1152D proband (arrow). Affected members are indicated by filled symbols. *B*, SSCP (single strand conformational polymorphism) analysis of exon 19 of the *SCN4A* gene showing an abnormal conformer that segregates with the disease. *C*, DNA sequence analysis of exon 19 demonstrating a transition from C to A at nucleotide 3455, which causes an A1152D mutation in the Na^+ channel α subunit. *D*, topology of the α subunit of the skeletal muscle Na^+ channel indicating the location of A1152D mutation in DIII/S4-S5 linker. Amino acid sequence alignments of DIII/S4–S5 of different sodium channels are represented below to demonstrate the conservation of alanine at position 1152 between isoforms and species (from Swissprot and TrEMBL databanks).

the corresponding A1152D point mutation (framed characters) had the following sequences: 5′-GTGGTGGTGAACGACCTCCTAGGCGCCATC-3′ (forward) and 5′-GATGGCGCCTAGGAGGTCGTTCAC-CACCAC-3′ (reverse). Each oligo-nucleotide was amplified with Pfu turbo DNA polymerase (Stratagene, La Jolla, California). The nicked vector containing the A1152D mutation was generated and transformed into *E. coli* (XL10-gold ultra-competent cells). Different clones were selected after digestion with *Sac*I, *Bam*HI and *Eco*RI restriction enzymes (Bouhours *et al.* 2004). The final construct used for cell transfection was sequenced entirely to verify the presence of the mutation, and ensure that no other variant was accidentally introduced during DNA amplification.

Transfection and cell culture

The pRc/CMV construct encoding either WT human Na^+ channel α-subunit or A1152D mutant was introduced into HEK293 cells using the calcium phosphate precipitation method. The presence of the *Neo* gene enabled selection of stably expressing clones by addition of geneticin (800 μg ml^{-1}, Gibco/BRL, USA) in the culture medium. Cell colonies were harvested after about 2 weeks, and Na^+ channel expression was verified by both RT-PCR, and electrophysiology. Only uniform colonies expressing peak sodium currents between 1 and 2 nA were kept for the electrophysiological study. Stably expressing cells were routinely grown at 37°C (5% CO_2, 95% humidity) in Dulbecco's modified Eagle's medium containing 10% fetal bovine serum and 250 μg ml^{-1} geneticin (Gibco/BRL, USA), to maintain the selection pressure. At least two different cell clones expressing the A1152D mutation were investigated.

Electrophysiology and data analysis

Whole-cell currents (Hamill *et al.* 1981) were recorded using an EPC-7 patch-clamp amplifier (List-Medical, Germany) and filtered through an 8-pole low-pass Bessel filter (M900, Frequency Devices, MA, USA). Signal acquisition and processing were performed using the DigiData card (1200 A) and pCLAMP (v8) software (Axon Instruments, Union City, CA, USA). In general, whole-cell currents were filtered at 5 kHz, and digitized at 20 or

50 μs sampling intervals. Tail currents, with faster kinetics, were recorded at the highest sampling rate (5 μs), and processed with and without filtering to exclude signal distortion. Low-pass filtering tail currents at 10 kHz usually improved signal to noise ratio, while preserving the kinetics. To minimize space-clamp problem, recordings were performed on small isolated round cells (10–20 μm diameter). After entering the whole-cell configuration, a period of several minutes was allowed before recording, to allow stabilization of Na^+ current amplitude. Cells were considered for analysis only if the leakage current remained insignificant throughout the experiment (holding current $<$0.1 nA at $-$100 mV). Capacitance and series resistance were compensated using the analog circuitry of the amplifier, and were verified throughout the experiment. Series resistance was compensated at $>$80%. For all the data presented herein, the access resistance and the ensuing voltage error had a maximum value of 3 MΩ and 3.5 mV, respectively. A P/N protocol (Bezanilla & Armstrong, 1977) was applied to subtract residual leakage and capacity currents. The number (4–8) and onset of subpulses, as well as the holding potential were adjusted to ensure that this subtraction process did not alter the data. Recordings were carried out either at 21°C (room temperature) or at 11 ± 1°C using a water-based heater-cooler (Thermomix 1441 and Frigomix 1495, B. Braun Melsungen., Germany), combined with water flow through a thermally conductive recording chamber. Bath temperature was recorded using two thermistors connected to a digital thermometer (Eirelec LTD, Ireland). Patch pipettes (2–2.5 MΩ) were pulled from borosilicate capillary glass (Drummond Scientific Co., Broomall, PA, USA) using a Sutter P-97 micropipette puller. For all recordings, except those concerning slow inactivation, the composition (mM) of the pipette and bath solutions were: 130 CsCl, 2 $MgCl_2$, 10 glucose and 0 Hemi-Sodium Hepes, pH 7.4 and 120 NaCl, 20 Choline-Cl, 3 KCl, 2 $MgCl_2$, 1 $CaCl_2$, 10 Glucose and 10 Hepes, pH 7.4, respectively. To prolong seal stability when slow inactivation protocols were applied, the pipette was filled with a fluoride based-solution (mM): 80 CsF, 35 NaCl, 10 EGTA, 24 CsOH and 10 Hepes, pH 7.4. The corresponding bath solution contained (mM): 150 NaCl, 2 KCl, 1 $MgCl_2$, 2 $CaCl_2$, 5 Glucose and 10 Hepes, pH 7.4. All solutions had an osmolarity between 300 and 320 mosmol l^{-1} . Chemicals were purchased from Sigma. Current analysis and data process were performed using pCLAMP 8.2, Excel (Microsoft) and Fig-P (Biosoft, Cambridge, UK) software.

Conductance was computed from the equation $G = I/(V - E_{rev})$ where I is the peak current at a given voltage V, and E_{rev} the equilibrium potential extrapolated from the graph. The voltage for half activation $V_{0.5}$ and the slope factor k were obtained by fitting the conductance–voltage curves to a Boltzmann distribution $G(V)/G_{max} = 1/(1 + \exp(-(V - V_{0.5})/k))$, where $G(V)$ is the sodium conductance at a given voltage V, G_{max} the maximum conductance. Steady-state inactivation curves were fitted to the equation $I(V)/I_{max} = 1/(1 + \exp((V - V_{0.5})/k))$, where $I(V)/I_{max}$ represents the current ratio, V the prepulse test voltage, and k the slope factor. Fast inactivation and deactivation time constants (τ) were determined by mono-exponential fitting of the macroscopic current decay using the equation $I = I_{resid} + A\exp(-t/\tau)$, where I symbolizes current intensity, I_{resid} the asymptotic residue and A the current amplitude at time zero. Data are expressed as mean ± S.E.M and the difference between two mean values was considered statistically significant when the P-value given by the unpaired student-t-test was lower than 0.05.

Results

Identification of A1152D mutation

Following PCR-SSCA analysis of the *SCN4A* gene, an abnormal conformer was found in exon 19 of PC patients. The primers used to amplify exon 19 and intron–exon boundaries were 5′-CTCTCTCAGAGGCTGGG-AGA-3′ (forward primer) and 5′-CTCCATCCAGGTT-CCCGGCA-3′ (reverse primer). Direct sequencing of exon 19 revealed a C to A transition at position 3455, predicting a substitution of the highly conserved alanine 1152 by aspartic acid in the sodium channel α subunit (Fig. 1*B*–*D*). An A1152D mutation was not found in 250 healthy adults from the same ethnic background as the patients (Caucasian) but unrelated to them.

Voltage dependence of channel activation

The effects of A1152D mutation were investigated in HEK cells that stably expressed A1152D or WT hSkM1 α subunits. Whole-cell Na^+ currents were evoked by a series of depolarizing steps ranging from $-$70 to +65 mV from a holding potential of $-$100 mV. Peak currents were scaled to the maximal amplitude for each cell, to yield normalized I–V curves. Using the same data and graphically determined reversal potentials, we calculated the Na^+ conductance for the various voltages applied (see Methods). Current–voltage (I–V) and conductance–voltage (G–V) curves obtained for A1152D mutant ($n = 25$) channels were perfectly superimposed to those obtained from the WT ($n = 17$) (Fig. 2*A* and *B*). G–V curves were fit to a standard Boltzmann distribution (see Methods). No statistically significant difference was found between the mean values (±S.E.M.) of the voltage for half activation $V_{0.5}$ (-18.66 ± 0.42 and -19.65 ± 0.70 mV) or the slope factor k (7.23 ± 0.13 and 7.39 ± 0.18 mV (e-fold change)$^{-1}$) obtained for A1152D mutant and WT, respectively. These results indicate

Table 1. Mean values (±S.E.M.) of the Boltzmann fits ($V_{0.5}$ and k) to activation and fast inactivation curves obtained for A1152D mutant and WT at 21°C and 11°C

			Activation		Fast inactivation		
		E_{rev} (mV)	$V_{0.5}$ (mV)	k (mV (e-fold change)$^{-1}$)	$V_{0.5}$ (mV)	k (mV (e-fold change)$^{-1}$)	I_{ss}/I_{peak} (%)
	Nernst	80.5					
21°C	A1152D	81.1 ± 0.9 (25)	−18.6 ± 0.4 (25)	7.2 ± 0.1 (25)	−65.7 ± 0.5 (8)	6.9 ± 0.2 (8)	0.96 ± 0.14 (5)
	WT	81.3 ± 0.8 (17)	−19.6 ± 0.7 (17)	7.3 ± 0.1 (17)	−71.3 ± 0.4 (10)	6.3 ± 0.3 (10)	0.78 ± 0.07 (6)
	Nernst	77.7					
11°C	A1152D	76.7 ± 0.4 (12)	−13.5 ± 0.4 (12)	8.2 ± 0.1 (12)	−64.8 ± 0.3 (10)	7.7 ± 0.4 (10)	4.42 ± 0.62 (7)
	WT	76.9 ± 0.6 (15)	−15.1 ± 0.4 (15)	8.2 ± 0.1 (15)	−73.7 ± 0.3 (11)	6.4 ± 0.3 (11)	1.55 ± 0.35 (9)

The last column indicates the fraction of sustained current ($I_{ss}/I_{peak} \times 100$) measured at the end of a 200 ms pulse to −10 mV.

that the A1152D mutation did not modify the voltage dependence of Na^+ channel activation. The mean value of the mutant reversal potential (81.19 ± 0.90 mV) was similar to that of the WT (81.33 ± 0.82 mV), and both were comparable to the Nernst value (−80.46 mV) (see Table 1).

Kinetics and voltage dependence of fast inactivation

Alterations of fast inactivation have been reported in most Na^+ channel mutants associated with PC. However, the degree and nature of these alterations vary between different mutants (Yang *et al.* 1994; Cannon, 1996). The effect of the A1152D mutation on channel fast inactivation kinetics was analysed by fitting the decay of the whole-cell current elicited at each potential with a single exponential, and comparing the values of the time constants (τ_h) between A1152D and WT. Mono-exponential fitting could be readily obtained at voltages ranging from −40 to +40 mV (Fig. 3*A*). To ensure full current decay and the best exponential fitting, we tested depolarizing steps of increasing durations from 20 to 200 ms. Over the whole voltage range, A1152D induced a 2–3-fold increase in the time constant as compared to the WT. For example, at −10 mV, the mean value ± S.E.M. of τ_h was 1.34 ± 0.05 ms ($n = 27$) and 0.69 ± 0.03 ms ($n = 17$) for A1152D and WT channels, respectively. The pattern of voltage dependence of τ_h was not modified by the mutation.

The voltage dependence of steady-state fast inactivation was studied using 500 ms prepulses ranging from −120 to +20 mV, followed by a 20 ms test pulse at −10 mV. The fraction of current recorded during the test pulse was plotted against the prepulse voltage for both mutant and WT channels. Figure 3*B* shows that the A1152D mutation shifted the voltage dependence of steady-state fast inactivation by 5 mV toward depolarization, without changing its steepness. Fitting each curve with a standard Boltzmann function yielded $V_{0.5}$ of −65.72 ± 0.50 mV ($n = 8$) and −71.31 ± 0.47 mV ($n = 10$) for A1152D and WT ($P < 0.001$), respectively. The slope factor remained unchanged with a mean value of 6.92 ± 0.27 for A1152D, and 6.37 ± 0.30 for the WT.

The recovery of Na^+ channels from fast inactivation was also investigated. The standard protocol consisted of a first depolarization at −10 mV for 60 ms to fully inactivate the channels, followed by increasing periods of membrane repolarization (1–320 ms), before a second depolarization of 20 ms at −10 mV to measure the fraction of current recovered. Different recovery potentials ranging from −140 to −80 mV in 10 mV increments were applied to determine the voltage dependence of channel recovery

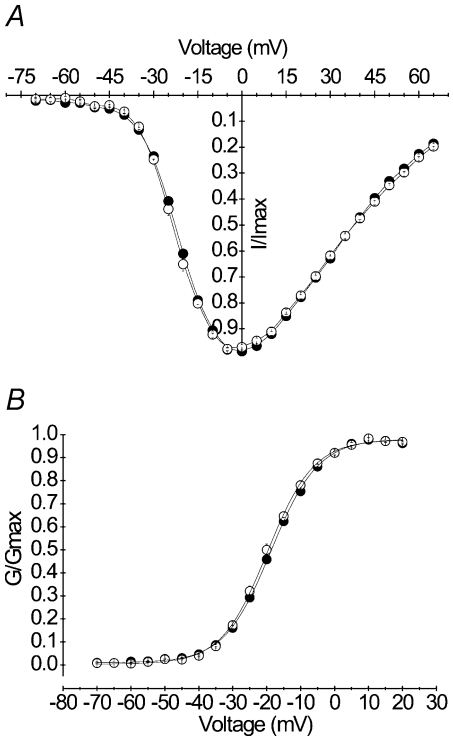

Figure 2. Voltage dependence of activation
A, normalized peak current *versus* voltage curves obtained from HEK cells expressing either A1152D (● $n = 27$) or WT (○ $n = 17$) Na^+ channels. Currents were evoked by a series of voltage steps ranging from −70 mV to +65 mV from a holding potential of −100 mV. *B*, steady-state activation: peak Na^+ conductance (G) was calculated from data shown in *A* (see Methods), and normalized to the maximal value (G_{max}). Both mutant and WT G/G_{max} *versus* voltage curves were fitted with a Boltzmann function as denoted by the continuous lines (see Table 1 for $V_{0.5}$ and k values).

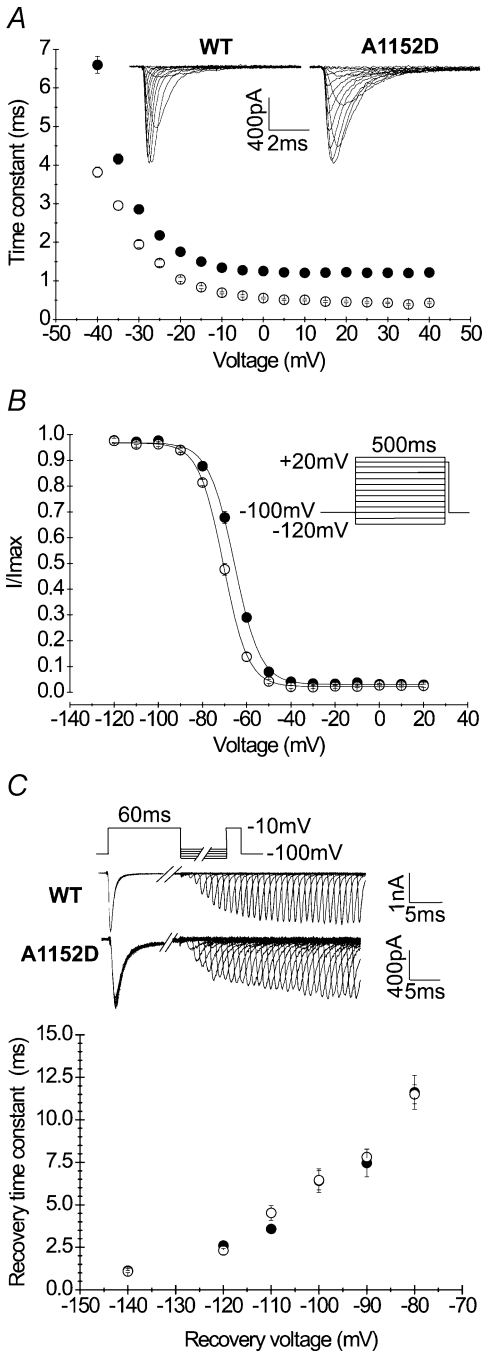

Figure 3. Kinetics and voltage dependence of fast inactivation
A, fast inactivation kinetics were measured from the exponential decay of whole-cell currents evoked by various membrane depolarization steps in HEK cells expressing A1152D (● $n = 27$) or WT (○ $n = 17$) Na^+ channels (holding potential: −100 mV). The inset shows representative tracings of superimposed Na^+ currents obtained at different potentials. Note the slower decay of A1152D currents compared with WT. *B*, steady-state fast inactivation curves: channels were inactivated using a series of 500 ms prepulses to various voltages, followed by a test pulse to −10 mV. Currents evoked during the test pulse were normalized to the maximal current usually following the most negative conditioning prepulse. Curves obtained for both A1152D (● $n = 8$) and WT (○ $n = 10$) Na^+ channels were readily fitted with a Boltzmann function (see Table 1 for $V_{0.5}$ and *k* values). Note the depolarizing shift of the mutant steady-state curve compared with that of the WT. *C*, recovery from fast inactivation of A1152D or WT. Na^+ channels was examined using the two-pulse protocol shown above the tracings. Recovery voltages ranged from −140 mV to −70 mV and recovery duration from 1 ms to 320 ms. Superimposed current tracings illustrate gradual recovery with time for a repolarizing potential of −100 mV. The fraction of recovered current *versus* repolarization time followed a single exponential. The recovery time constant *versus* recovery voltage curves of the mutant (● $n = 5$–7) and WT (○ $n = 7$) are shown in the lower graph.

from fast inactivation. The increase in the fraction of current recovered with the repolarizing periods followed a single exponential function whose time constant is plotted against the recovery voltages. The results shown in Fig. 3*D* indicate that the A1152D did not modify Na^+ channel recovery from fast inactivation at the tested voltages.

Sustained current

Whole-cell Na^+ currents recorded from HEK cells expressing the WT *SCN4A* gene exhibit a small sustained component whose magnitude depends on the recording conditions (Cummins *et al.* 1993). In our hands, the sustained current was barely detectable in cells expressing WT channels. In PC mutants, an increase in the sustained current (I_{ss}) has been implicated in the pathogenesis of myotonia. To assess the contribution of the sustained current in A1152D mutants, we first determined the time necessary for the Na^+ current to reach the steady level. Hence, we measured the current at various depolarization times ranging from 20 to 500 ms. We found that for both mutant and WT, whole-cell currents reached a steady value around 100 ms depolarization. Measurements of the fraction of sustained current (I_{ss}/I_{peak}) showed no difference between mutant or WT when performed at the end of depolarizing pulses lasting 100 ms or longer. The mean values of I_{ss}/I_{peak} obtained at various voltages in both mutant and WT are illustrated in Fig. 4. The fraction of sustained current was similar in mutant ($n = 5$) and WT ($n = 6$) and ranged from 0.7 to 2.5% of the peak between −20 and +40 mV.

Voltage dependence and kinetics of slow inactivation

Slow inactivation is a process by which a number of voltage-gated channels become non-conducting following prolonged membrane depolarization. Na^+ channel slow inactivation occurs in an order of tens of seconds, and is thought to regulate the number of available channels as a function of slow variations in the membrane potential (Simoncini & Stuhmer, 1987; Ruff *et al.* 1988; Ruff, 1999). Although *SCN4A* mutations affecting slow inactivation generally produce muscle paralysis rather than myotonia (Hayward *et al.* 1997; Hayward *et al.*

1999), the involvement of the S4–S5 region in this process (Bendahhou *et al.* 2002) led us to analyse the effect of the A1152D mutation on channel slow inactivation. Besides, the structural basis of slow inactivation is still unclear, and may benefit from systematic studies of naturally occurring mutations.

The onset and the voltage dependence of slow inactivation were compared between mutant and WT channels. To induce channel entry into slow inactivation, depolarizing pulses to −10 mV were applied for increasing periods ranging from 1 ms to 100 s (Fig. 5*A*, inset). Each pulse was successively followed by a short repolarization (−100 mV, 20 ms) to selectively remove fast inactivation, and by a test pulse (−10 mV, 20 ms) to estimate the fraction of slow inactivated channels. As shown in Fig. 5*A*, there was no difference in the kinetics of entry into slow inactivation between mutant and WT. In both cases, the kinetics of entry into slow inactivation followed a mono-exponential function with comparable time constants (1.48 ± 0.23 s ($n = 5$) and 1.44 ± 0.14 s ($n = 5$) for A1152D and WT, respectively).

The voltage dependence of steady-state slow inactivation was assessed using a series of 50 s pulses from −130 mV to +30 mV, followed successively by a short repolarization to −100 mV for 20 ms to remove fast inactivation, and a test pulse to −10 mV for 20 ms to estimate the fraction of slow inactivated current. To prevent accumulation of slow inactivation, cells were maintained at the holding potential (−100 mV) for 50 s between successive depolarizing episodes of the series. Steady-state slow inactivation curves (s_∞) obtained for both mutant and WT channels were readily fitted to a Boltzmann function (see Methods). As can be seen from Fig. 5*C*, curves plotted for both channel types were superimposed and none of the Boltzmann fits was modified by the mutation. The mean values of $V_{0.5}$ and k were -66.14 ± 2.20 mV and 6.72 ± 0.51 ($n = 7$) for the mutant, and -66.91 ± 1.16 mV and 7.43 ± 0.32 ($n = 6$) for the WT. These data indicate that the A1152D mutation has no effect on the voltage dependence of Na^+ channel slow inactivation.

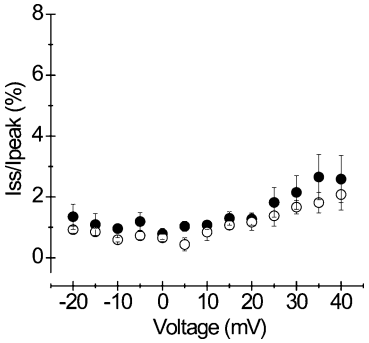

Figure 4. Sustained current
Current–voltage relationship of the sustained component for A1152D (● $n = 5$) and WT (○ $n = 6$). The sustained current (I_{ss}) was measured at the end of 200 ms pulses and its relative value to the peak (in percentage) was plotted against the voltage (−20 to +40 mV). Note that there was no difference in the sustained current under standard recording conditions (21°C).

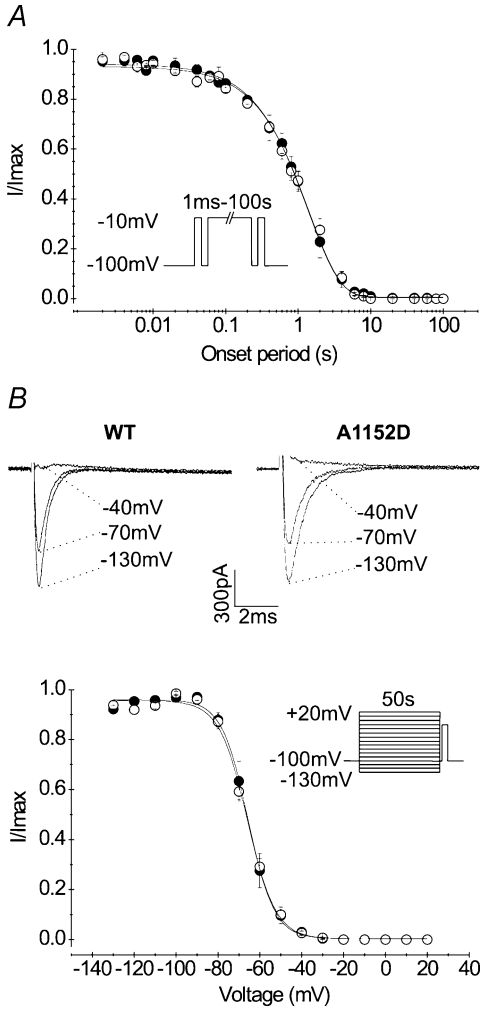

Figure 5. Voltage dependence and kinetics of slow inactivation
A, the onset of slow inactivation for A1152D mutant (● $n = 5$) and WT (○ $n = 5$) was studied using the protocol shown in the inset. Briefly, cells were depolarized for increasing periods (0.001–100 s) to determine the kinetics of entry into slow inactivation. This conditioning pulse was preceded by a reference and followed by a test pulse to −10 mV for 20 ms. Prior to the test, a short repolarization was applied to enable full recovery from fast inactivation. Changes of the fraction of slow inactivated current (I/I_{ref}) with time followed a monoexponential function with similar time constants for mutant ($n = 5$) and WT ($n = 5$). *B*, steady-state slow inactivation curves obtained for the mutant (● $n = 7$) and the WT (○ $n = 6$) using the protocol shown in the inset. The upper tracings illustrate the voltage-dependent decrease in Na^+ current induced by channel slow inactivation (capacitive currents blanked). Steady-state curves were fitted with a Boltzmann function with the following parameters for A1152D mutant and WT, respectively: $V_{0.5}$: -65.4 ± 2.3 and $V_{0.5}$: -66.9 ± 1.1 mV, k: 6.7 ± 0 5 and 7.4 ± 0.3 mV (e-fold change)$^{-1}$).

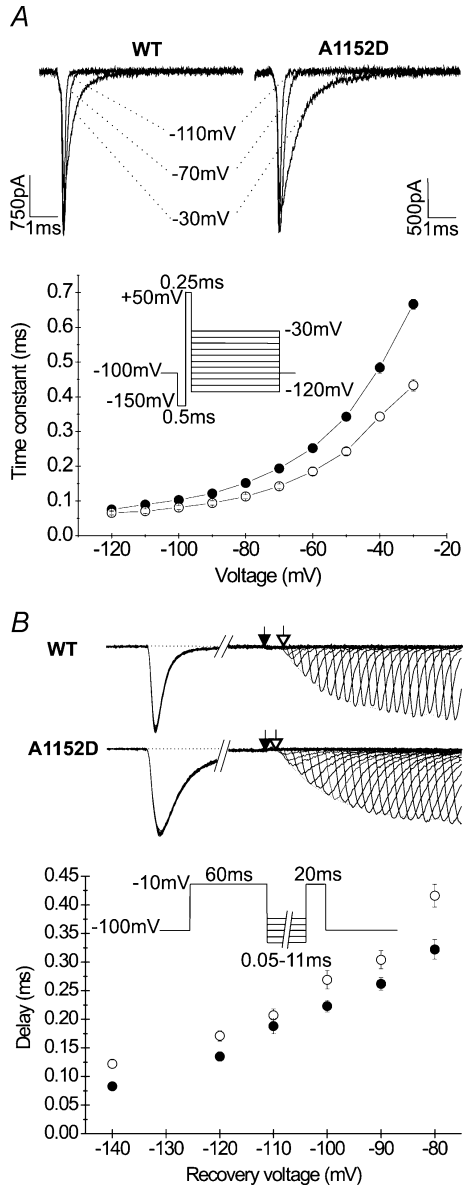

Figure 6. Deactivation from open and inactivated states
A, representative traces of tail currents obtained using the protocol shown below. The kinetics of Na^+ channel deactivation from the open state were assessed from the time constant of the monoexponential decay of the tail current. The graph compares the deactivation time constant *versus* voltage curves obtained for the mutant (● $n = 6$) and WT (○ $n = 6$). Note that the difference between the two curves indicating a slowing of the tail current decay for the mutant is only noticeable at potentials positive to −80 mV. *B*, deactivation from the inactivated state was assessed via the delay in the onset to recovery from fast inactivation. The upper tracings are typical recordings obtained using the protocol shown underneath, with different repolarizing potentials of increasing duration (from 0.05 to 11 ms). The fraction of recovered peak currents followed an exponential growth with time of recovery (broken line). The delay to recovery was measured between the end of the depolarizing pulse (filled arrow) and intersection of the exponential curve with the base line (open arrow). The curves show the voltage dependence of the delay for A1152D mutants (● $n = 6$–8) and WT (○ $n = 8$). Note the shorter delay in the onset to recovery for the mutant as compared to the WT, indicating accelerated deactivation from the inactivated state at all voltages tested.

Deactivation from the open and from the inactivated states

Several PC mutations have been shown to impair Na^+ channel deactivation, with a correlation between the degree of impairment and the severity of the phenotype (Featherstone *et al.* 1998). Furthermore, conserved residues in the S4–S5 linker of different domains have been shown to slow the rates of Na^+ channel deactivation (Richmond *et al.* 1997). We studied the effects of A1152D mutation on the kinetics of Na^+ channel deactivation from the open and from the inactivated states. To assess deactivation from the open state, cells were first hyperpolarized to −150 mV to fully remove fast inactivation, and then briefly stepped to +50 mV (250 μs), before a series of repolarizing pulses ranging from −120 to −30 mV was applied to induce channel deactivation. Tail currents evoked by membrane repolarization decayed with a single exponential function whose time constant was used to quantify deactivation kinetics. Changes of the deactivation time constants (τ_D) with the voltage are shown in Fig. 6*A*. At voltages negative to −60 mV mean values of τ_D obtained from the mutant were not statistically different from those compiled from the WT. For weaker repolarization (between −60 and −30 mV), mutant values diverged from the WT. However, at these voltages, tail current may also reflect fast inactivation (Cota & Armstrong, 1989; Featherstone *et al.* 1998), and the slowed current decay may be attributed to the slowing of fast inactivation rates.

In skeletal muscle Na^+ channels, macroscopic recovery from fast inactivation proceeds after a delay that shortens with increasing repolarization. The delay in the onset to recovery reflects channel deactivation from the inactivated state, indicating that these channels must deactivate before they recover from fast inactivation. Such coupling between deactivation and inactivation prevents resurgent current upon recovery, and implies steep voltage dependence for both processes (Kuo & Bean, 1994). Deactivation from the inactivated state was assessed from the delay in the onset to recovery using a recovery protocol with 60 ms prepulses to enable full inactivation, and short repolarizing increments to better resolve the recovery delay. The delay was measured from the zero intercept of the single exponential function that fitted the recovered peak current intensity. As shown in Fig. 5*B*, the delay in the onset to recovery was decreased in the A1152D mutant ($n = 6$–8) as compared to the WT ($n = 8$). This decrease was present over the whole range of voltage tested (from −140 to −80 mV), but was more pronounced at −80 mV.

Effect of cold

One of the typical features of PC is the sensitivity of myotonia to cold. To understand the molecular mechanism underlying this temperature sensitivity, we

have examined the effect of 10°C cooling on A1152D channel activation, deactivation, fast inactivation and on I_{ss}. Cooling is generally known to slow down Na^+ channel gating, and has been shown to enhance Na^+ channel slow inactivation, reducing thereby the number of channels available for excitation (Ruff, 1999). However, since slow inactivation was not affected by the A1152D mutation, we did not examine its changes with decreasing temperature.

Our data show that a 10°C cooling from the normal recording temperature (21°C) causes a depolarizing shift in the voltage dependence of activation that was comparable between mutant (+ 5 mV) and WT (+ 4.5 mV) (Fig. 7). Boltzmann fits of the *G–V* curves and reversal potentials obtained at 21 and 11°C are depicted in Table 1. Note that the slope factors of the activation curves compiled at 11°C were not significantly different from those obtained at 21°C, and remained similar between mutant and WT.

Decreasing temperature induced a significant slowing of channel fast inactivation kinetics in both mutant and WT. To ensure accurate measurement of τ_h, we applied long depolarizing pulses of 500 ms duration that enabled full inactivation of Na^+ currents. Cooling from 21 to 11°C induced 5–7-fold increase of τ_h in the mutant as compared to 2–5-fold in the WT, indicating a higher temperature sensitivity of τ_h in the mutant. Figure 8*B* depicts changes of τ_h as a function of voltage for A1152D and WT channels at 21 and 11°C. One can notice that the data obtained for the mutant at low temperature were clearly out of the range delimited by the three other groups. Steady-state fast inactivation curves of both mutant and WT were not modified by cooling (Fig. 8*C*), and displayed a difference of 5 mV in $V_{0.5}$, similar to that observed at room temperature (see Table 1 for mean values of $V_{0.5}$ and k).

At 11°C, sustained currents (I_{ss}) were assessed at the end of 200 ms pulses to ensure steady current levels for both mutant and WT. This choice was based on prior tests using depolarizing pulses of varying durations from 40 to 500 ms to determine the most appropriate protocol for measuring I_{ss} under these conditions. Sustained to peak current ratio (I_{ss}/I_{peak}) *versus* voltage curves are represented in Fig. 9. Our results show that decreasing temperature increased I_{ss}/I_p in both mutant and WT. However, this effect was more pronounced for the mutant than for the WT. Between −20 and +40 mV, the maximum fraction of I_{ss} measured at 11°C reached about 6% of the peak in the mutant, and 4% in the WT as opposed to 2.5% at 21°C for both channels.

To study channel deactivation kinetics from the open state at 11°C, we used protocols in which the repolarizing pulse was increased to 25 ms to enable full tail current decay and, hence, reliable measurements of the deactivation time constant. The slowing of open state deactivation kinetics at decreased temperature provided a better resolution for disclosing differences between mutant and WT. Indeed, the small difference in τ_d observed at 21°C between the two channel types for the most negative potentials was enlarged at 11°C, and became statistically significant, indicating some subtle slowing of mutant channel deactivation from the open state. Comparison of the mean values of the deactivation time constant obtained at potentials negative to −70 mV yielded $P < 0.001$ between −70 and −110 mV, and $P < 0.01$ for −120 mV. Overall, decreasing temperature increased the deactivation time constant by 2–6-fold for the mutant and by 1.5–3.5-fold for the WT (Fig. 10), and enlarged the differences observed at 21°C for positive potentials.

Discussion

The present study focuses on the biophysical consequences of A1152D, a newly identified mutation in the S4–S5 linker of the skeletal muscle Na^+ channel α subunit causing paramyotonia congenita. To elucidate the gating defects of the A1152D mutant, we performed a thorough analysis of the macroscopic Na^+ current using HEK cells that stably express WT or A1152D hSkM1 channels. Our data show that this mutation induces mainly an impairment of fast inactivation, and accelerates deactivation from the

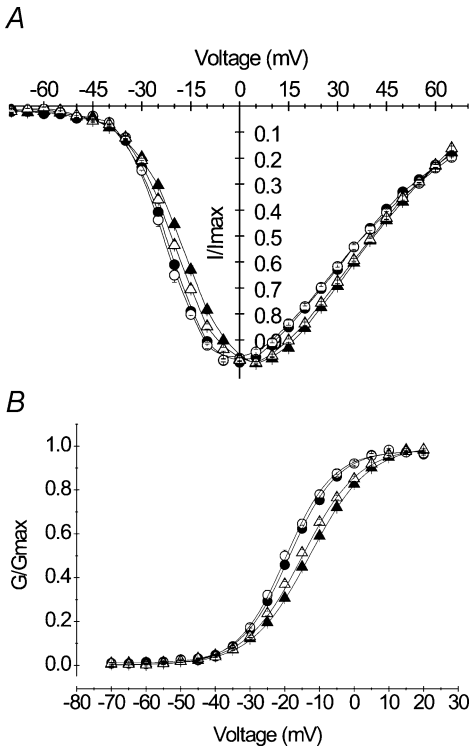

Figure 7. Effect of 10°C cooling on the voltage dependence of activation

A, current–voltage and *B*, conductance–voltage relationships obtained for A1152D (filled symbols) and WT (open symbols) at 21°C (● $n = 27$ or ○ $n = 17$) and 11°C (▲ $n = 12$ or △ $n = 11$). Recordings were performed according to usual voltage protocols (see Fig. 2). Note that cooling induced a 5 mV depolarizing shift in the voltage dependence of activation for both channel types.

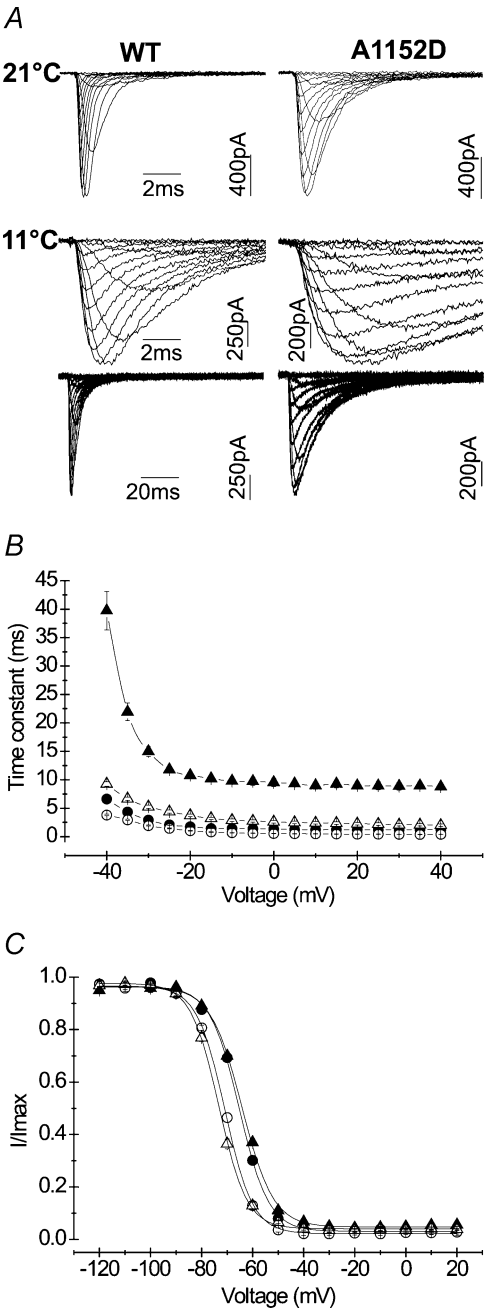

Figure 8. Effect of 10°C cooling on the kinetics and voltage dependence of fast inactivation
A, representative tracings of Na^+ currents recorded at 21°C (upper line) or 11°C (middle and lower lines). Note the different time scales used to display full current decay at 11°C (*B*). The different curves show changes of the fast inactivation time constant with the voltage at 21°C (● A1152D ($n = 27$), ○ WT ($n = 17$)) and 11°C (▲ A1152D ($n = 12$), △ WT ($n = 11$)). Long depolarizing steps were applied to ensure complete inactivation at 11°C. Note the significant slowing of the fast inactivation kinetics with cooling for both channels. However, the increase in the time constant with cooling was more pronounced for the mutant (5–7-fold) than for the WT (2–5-fold). Note that the curve representing the mutant at 11°C is clearly out of the range delimited by the three other groups (WT at both temperatures and A1152D at 21°C). *C*, steady-state fast inactivation curves obtained at 11°C (A1152D: ▲ $n = 10$; WT: △ $n = 11$) and superimposed to those obtained at 21°C (A1152D: ● $n = 8$; WT: ○ $n = 10$). Boltzmann fits remained unchanged with cooling, and did not remain comparable between A1152D mutant and WT.

inactivated state. Slow inactivation of A1152D mutant channels is normal. In the following discussion, we will consider both the molecular implications of A1152D channel biophysical properties, and the consequences on membrane excitability, especially at low temperature.

The A1152D mutation did not modify the voltage dependence of Na^+ channel activation. Mutagenesis of the homologous residue in the rat brain type II Na^+ channel α subunit (A1239) showed that A to K/Q/D substitution produced a small depolarizing shift of the voltage dependence of activation. The least change (about 2 mV) was observed for the A1239D mutant (Smith & Goldin, 1997). In hSkM1, A to C substitution at position 1152 did not induce any significant change in the voltage dependence of activation (Popa *et al.* 2004). Altogether, these data argue for a minor role of the central alanine of DIII/S4–S5 in Na^+ channel activation. It is worth noting that the voltage dependence of Na^+ channel activation was not affected by A1156T and I1160V, two point mutations in the same linker, known to cause hyperPP and PAM, respectively (Ptacek *et al.* 1994; Yang *et al.* 1994; Richmond *et al.* 1997). By contrast, hydrophobic residues in DII/S4–S5 have been shown to influence channel activation. This is clearly exemplified by two other mutations of hSkM1, L689I (hyperPP) and I693T (the A1152 counterpart in DII causing PC/hyperPP), which both induce a hyperpolarizing shift in the voltage dependence of activation (Plassart-Schiess *et al.* 1998; Bendahhou *et al.* 2002).

To date, most of the mutations associated with a clear-cut phenotype of PC have been shown to interfere with channel fast inactivation rather than channel activation (Yang *et al.* 1994; Cannon, 2000). The A1152D mutation disrupted Na^+ channel fast inactivation by slowing the kinetics, and shifting the voltage dependence of the steady-state toward depolarization. The sustained current was similar to the WT, and recovery from fast inactivation was not modified at voltages negative to −80 mV. All these macroscopic changes indicate that the A1152D mutation impairs channel inactivation presumably by affecting the transition from the open to the inactivated state (McPhee *et al.* 1998; Catterall, 2000). Inactivation from the closed state seems to be less affected by this mutation since at potentials negative to −70 mV, both steady-state and recovery curves were not significantly different from those of the WT. If, as suggested by Smith & Goldin (1997), the central alanine in DIII/S4–S5 represents a key element in the docking site for the inactivation particle, then, by eliminating a hydrophobic receptor site, the A1152D mutation would affect

fast inactivation by weakening the interaction with the IFM motif (West *et al.* 1992).

When assessed at 21°C, A1152D mutant channels displayed a very slight slowing of deactivation from the open state that was not statistically significant, and a clear acceleration of channel deactivation from the fast inactivated state compared with WT (Kuo & Bean, 1994). The voltage dependence of both transitions remained intact. Dissimilar effects of a given mutation of hSkM1 on open and inactivated state deactivation have been previously reported (Ji *et al.* 1996; Groome *et al.* 1999). Besides, mutant channels with disrupted fast inactivation often show a decrease in the delay to the recovery from inactivation, presumably because of less constraint for back movement of the activation gate (Groome *et al.* 1999; Bouhours *et al.* 2004).

The voltage dependence and the kinetics of entry into slow inactivation remained intact in A1152D mutant channels. In contrast, disease-associated mutations of topologically related residues in the DII/S4-S5 linker (L689I, I693T) have a major effect on channel slow inactivation, as opposed to their insignificant effect on fast inactivation. They also produce phenotypes characterized by episodes of muscle paralysis (Hayward *et al.* 1997; Plassart-Schiess *et al.* 1998; Hayward *et al.* 1999; Bendahhou *et al.* 2002). Again, this points to distinct roles of hydrophobic residues in S4–S5 linkers of DII and III, and corroborates the minor implication of slow inactivation in myotonia as opposed to muscle paralysis.

The A1152D mutation causes a clear-cut phenotype of PC characterized by cold-aggravated muscle stiffness. Our biophysical data are in line with previous reports showing that disruption of Na^+ channel fast inactivation represents a common pathogenic factor for PC (Yang *et al.* 1994; Hayward *et al.* 1996). Slowed rates of fast inactivation of A1152D channels will tend to hinder membrane repolarization during the action potential, thereby facilitating the occurrence of repetitive firing. As already reported for other PC-associated mutants, cooling further slowed inactivation and deactivation kinetics without changing their pattern of voltage dependence (Hayward *et al.* 1996; Bouhours *et al.* 2004; Dice *et al.* 2004). Our data also suggest a higher temperature sensitivity of τ_h and plausibly of the sustained current for the A1152D mutant compared with WT. Overall, by further slowing channel gating and enhancing the sustained current, cooling aggravated mutant channels defects and hence, their consequences on membrane excitability.

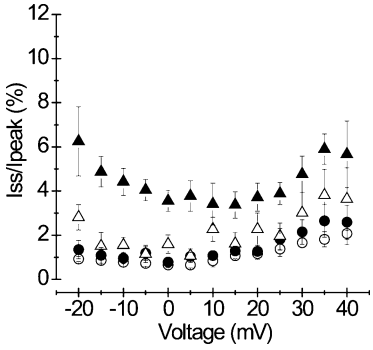

Figure 9. Effect of 10°C cooling on the sustained current
I_{ss}/I_{peak} *versus* voltage curves obtained at 11°C were superimposed with those obtained at 21°C for comparison: A1152D (● $n = 5$ at 21°C and ▲ n = 7 at 11°C) and WT (○ $n = 6$ at 21°C and △ n = 7 at 11°C). Sustained currents were measured using 200 ms depolarizing pulses (see Fig. 1 legend). Note that cooling increased the fraction of sustained current in both mutant and WT. However, as indicated by the difference that appears between mutant and WT, such effect was more pronounced for the mutant.

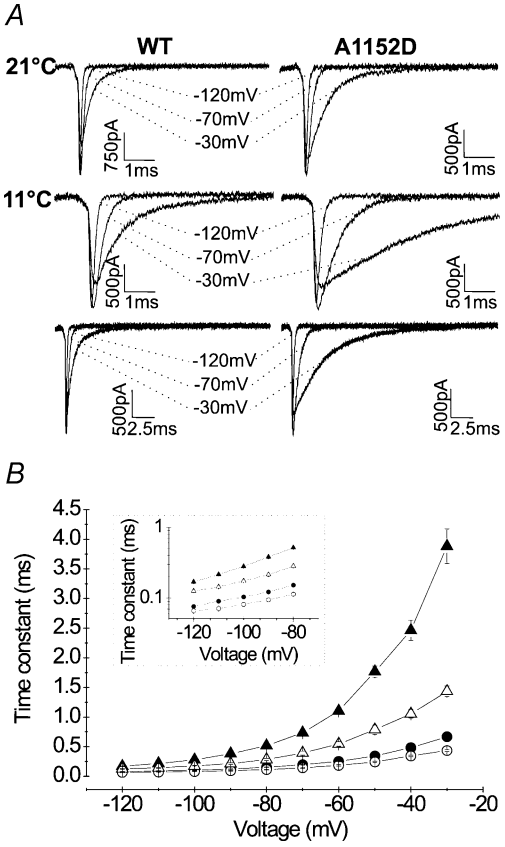

Figure 10. Effect of 10°C cooling on open-state deactivation kinetics
A, representative tail current tracings showing the drastic slowing of the tail current decay with decreasing temperature from 21°C (upper traces) to 11°C (middle and lower traces). To obtain full decay of the tail current and hence, accurate measurements of the deactivation time constant, the duration of the test pulse was prolonged to 25 ms when recordings were performed at 11°C. *B*, deactivation time constants *versus* voltage obtained at 11°C (△ WT $n = 5$; ▲ A1152D $n = 6$) and superimposed to those obtained at 21°C (○ WT $n = 5$; ● A1152D $n = 6$) for comparison. As evidenced by the logarithmic scale in the inset, cooling by 10°C exacerbated the differences between WT and mutant, unveiling slower deactivation at negative potentials.

In conclusion, this study defines the biophysical defects of a new Na^+ channel mutant associated with paramyotonia congenita, and shows their aggravation with cold. It also points to domain-specific roles of S4–S5 linkers, especially evidenced by distinct functional and phenotypic consequences of hydrophobic S4–S5 residues in domains II and III of hSkM1.

References

Bendahhou S, Cummins TR, Kula RW, Fu YH & Ptacek LJ (2002). Impairment of slow inactivation as a common mechanism for periodic paralysis in DIIS4–S5. *Neurology* **58**, 1266–1272.

Bezanilla F & Armstrong CM (1977). Inactivation of the sodium channel. I. Sodium current experiments. *J Gen Physiol* **70**, 549–566.

Bouhours M, Sternberg D, Davoine CS, Ferrer X, Willer JC, Fontaine B & Tabti N (2004). Functional characterization and cold sensitivity of T1313A, a new mutation of the skeletal muscle sodium channel causing paramyotonia congenita in humans. *J Physiol* **554**, 635–647.

Cannon SC (1996). Sodium channel defects in myotonia and periodic paralysis. *Annu Rev Neurosci* **19**, 141–164.

Cannon SC (2000). Spectrum of sodium channel disturbances in the nondystrophic myotonias and periodic paralyses. *Kidney Int* **57**, 772–779.

Cannon SC & Strittmatter SM (1993). Functional expression of sodium channel mutations identified in families with periodic paralysis. *Neuron* **10**, 317–326.

Catterall WA (2000). From ionic currents to molecular mechanisms: the structure and function of voltage-gated sodium channels. *Neuron* **26**, 13–25.

Chahine M, George AL Jr, Zhou M, Ji S, Sun W, Barchi RL & Horn R (1994). Sodium channel mutations in paramyotonia congenita uncouple inactivation from activation. *Neuron* **12**, 281–294.

Cota G & Armstrong CM (1989). Sodium channel gating in clonal pituitary cells. The inactivation step is not voltage dependent. *J Gen Physiol* **94**, 213–232.

Cummins TR, Zhou J, Sigworth FJ, Ukomadu C, Stephan M, Ptacek LJ & Agnew WS (1993). Functional consequences of a Na^+ channel mutation causing hyperkalemic periodic paralysis. *Neuron* **10**, 667–678.

Dice MS, Abbruzzese JL, Wheeler JT, Groome JR, Fujimoto E & Ruben PC (2004). Temperature-sensitive defects in paramyotonia congenita mutants R1448C and T1313M. *Muscle Nerve* **30**, 277–288.

Featherstone DE, Fujimoto E & Ruben PC (1998). A defect in skeletal muscle sodium channel deactivation exacerbates hyperexcitability in human paramyotonia congenita. *J Physiol* **506**, 627–638.

Filatov GN, Nguyen TP, Kraner SD & Barchi RL (1998). Inactivation and secondary structure in the D4/S4–5 region of the SkM1 sodium channel. *J Gen Physiol* **111**, 703–715.

Fleischhauer R, Mitrovic N, Deymeer F, Lehmann-Horn F & Lerche H (1998). Effects of temperature and mexiletine on the F1473S Na^+ channel mutation causing paramyotonia congenita. *Pflugers Arch* **436**, 757–765.

Fontaine B, Khurana TS, Hoffman EP, Bruns GA, Haines JL, Trofatter JA, Hanson MP, Rich J, McFarlane H, Yasek DM & *et al.* (1990). Hyperkalemic periodic paralysis and the adult muscle sodium channel alpha-subunit gene. *Science* **250**, 1000–1002.

Fournier E, Arzel M, Sternberg D, Vicart S, Laforet P, Eymard B, Willer JC, Tabti N & Fontaine B (2004). Electromyography guides toward subgroups of mutations in muscle channelopathies. *Ann Neurol* **56**, 650–661.

George AL Jr, Komisarof J, Kallen RG & Barchi RL (1992). Primary structure of the adult human skeletal muscle voltage-dependent sodium channel. *Ann Neurol* **31**, 131–137.

Groome JR, Fujimoto E, George AL & Ruben PC (1999). Differential effects of homologous S4 mutations in human skeletal muscle sodium channels on deactivation gating from open and inactivated states. *J Physiol* **516**, 687–698.

Hamill OP, Marty A, Neher E, Sakmann B & Sigworth FJ (1981). Improved patch-clamp techniques for high-resolution current recording from cells and cell-free membrane patches. *Pflugers Arch* **391**, 85–100.

Hayward LJ, Brown RH Jr & Cannon SC (1996). Inactivation defects caused by myotonia-associated mutations in the sodium channel III–IV linker. *J Gen Physiol* **107**, 559–576.

Hayward LJ, Brown RH Jr & Cannon SC (1997). Slow inactivation differs among mutant Na channels associated with myotonia and periodic paralysis. *Biophys J* **72**, 1204–1219.

Hayward LJ, Sandoval GM & Cannon SC (1999). Defective slow inactivation of sodium channels contributes to familial periodic paralysis. *Neurology* **52**, 1447–1453.

Hille B (1982). Membrane excitability: Action potential and ionic channels. In *Physiology and Biophysics*, 20th edn, vol. IV, ed. Ruch TC & Patton E, pp. 68–100. W.B. Saunders, Philadelphia.

Ji S, George AL Jr, Horn R & Barchi RL (1996). Paramyotonia congenita mutations reveal different roles for segments S3 and S4 of domain D4 in hSkM1 sodium channel gating. *J General Physiol* **107**, 183–194.

Jurkat-Rott K, Mitrovic N, Hang C, Kouzmekine A, Iaizzo P, Herzog J, Lerche H, Nicole S, Vale-Santos J, Chauveau D, Fontaine B & Lehmann-Horn F (2000). Voltage-sensor sodium channel mutations cause hypokalemic periodic paralysis type 2 by enhanced inactivation and reduced current. *Proc Natl Acad Sci U S A* **97**, 9549–9554.

Koch MC, Baumbach K, George AL & Ricker K (1995). Paramyotonia congenita without paralysis on exposure to cold: a novel mutation in the SCN4A gene (Val1293Ile). *Neuroreport* **6**, 2001–2004.

Kuo CC & Bean BP (1994). Na^+ channels must deactivate to recover from inactivation. *Neuron* **12**, 819–829.

Lehmann-Horn F, Jurkat-Rott K & Rudel R (2002). Periodic paralysis: understanding channelopathies. *Curr Neurol Neurosci Rep* **2**, 61–69.

Lerche H, Peter W, Fleischhauer R, Pika-Hartlaub U, Malina T, Mitrovic N & Lehmann-Horn F (1997). Role in fast inactivation of the IV/S4–S5 loop of the human muscle Na^+ channel probed by cysteine mutagenesis. *J Physiol* **505**, 345–352.

McClatchey AI, McKenna-Yasek D, Cros D, Worthen HG, Kuncl RW, DeSilva SM, Cornblath DR, Gusella JF & Brown RH Jr (1992*a*). Novel mutations in families with unusual and variable disorders of the skeletal muscle sodium channel. *Nat Genet* **2**, 148–152.

McClatchey AI, Van den Bergh P, Pericak-Vance MA, Raskind W, Verellen C, McKenna-Yasek D, Rao K, Haines JL, Bird T & Brown RH Jr (1992*b*). Temperature-sensitive mutations in the III–IV cytoplasmic loop region of the skeletal muscle sodium channel gene in paramyotonia congenita. *Cell* **68**, 769–774.

McPhee JC, Ragsdale DS, Scheuer T & Catterall WA (1998). A critical role for the S4–S5 intracellular loop in domain IV of the sodium channel alpha-subunit in fast inactivation. *J Biol Chem* **273**, 1121–1129.

Mitrovic N, Lerche H, Heine R, Fleischhauer R, Pika-Hartlaub U, Hartlaub U, George AL Jr & Lehmann-Horn F (1996). Role in fast inactivation of conserved amino acids in the IV/S4–S5 loop of the human muscle Na^+ channel. *Neurosci Lett* **214**, 9–12.

Miyamoto K, Nakagawa T & Kuroda Y (2001). Solution structures of the cytoplasmic linkers between segments S4 and S5 (S4–S5) in domains III and IV of human brain sodium channels in SDS micelles. *J Pept Res* **58**, 193–203.

Mohammadi B, Mitrovic N, Lehmann-Horn F, Dengler R & Bufler J (2003). Mechanisms of cold sensitivity of paramyotonia congenita mutation R1448H and overlap syndrome mutation M1360V. *J Physiol* **547**, 691–698. Epub 2003 January 2024.

Plassart E, Eymard B, Maurs L, Hauw JJ, Lyon-Caen O, Fardeau M & Fontaine B (1996). Paramyotonia congenita: genotype to phenotype correlations in two families and report of a new mutation in the sodium channel gene. *J Neurol Sci* **142**, 126–133.

Plassart-Schiess E, Lhuillier L, George AL Jr, Fontaine B & Tabti N (1998). Functional expression of the Ile693Thr Na^+ channel mutation associated with paramyotonia congenita in a human cell line. *J Physiol* **507**, 721–727.

Popa MO, Alekov AK, Bail S, Lehmann-Horn F & Lerche H (2004). Cooperative effect of S4–S5 loops in domains D3 and D4 on fast inactivation of the Na^+ channel. *J Physiol* **561**, 39–51. Epub 2004 September 2030.

Ptacek L (1998). The familial periodic paralyses and nondystrophic myotonias. *Am J Med* **105**, 58–70.

Ptacek LJ, George AL Jr, Barchi RL, Griggs RC, Riggs JE, Robertson M & Leppert MF (1992). Mutations in an S4 segment of the adult skeletal muscle sodium channel cause paramyotonia congenita. *Neuron* **8**, 891–897.

Ptacek LJ, Tawil R, Griggs RC, Meola G, McManis P, Barohn RJ, Mendell JR, Harris C, Spitzer R, Santiago F & *et al.* (1994). Sodium channel mutations in acetazolamide-responsive myotonia congenita, paramyotonia congenita, and hyperkalemic periodic paralysis. *Neurology* **44**, 1500–1503.

Richmond JE, VanDeCarr D, Featherstone DE, George AL Jr & Ruben PC (1997). Defective fast inactivation recovery and deactivation account for sodium channel myotonia in the I1160V mutant. *Biophys J* **73**, 1896–1903.

Ruff RL (1999). Effects of temperature on slow and fast inactivation of rat skeletal muscle Na^+ channels. *Am J Physiol Cell Physiol* **277**, C937–C947.

Ruff RL, Simoncini L & Stuhmer W (1988). Slow sodium channel inactivation in mammalian muscle: a possible role in regulating excitability. *Muscle Nerve* **11**, 502–510.

Simoncini L & Stuhmer W (1987). Slow sodium channel inactivation in rat fast-twitch muscle. *J Physiol* **383**, 327–337.

Smith MR & Goldin AL (1997). Interaction between the sodium channel inactivation linker and domain III, S4–S5. *Biophys J* **73**, 1885–1895.

Tang L, Kallen RG & Horn R (1996). Role of an S4–S5 linker in sodium channel inactivation probed by mutagenesis and a peptide blocker. *J Gen Physiol* **108**, 89–104.

West JW, Patton DE, Scheuer T, Wang Y, Goldin AL & Catterall WA (1992). A cluster of hydrophobic amino acid residues required for fast Na^+-channel inactivation. *Proc Natl Acad Sci U S A* **89**, 10910–10914.

Yang N, Ji S, Zhou M, Ptacek LJ, Barchi RL, Horn R & George AL Jr (1994). Sodium channel mutations in paramyotonia congenita exhibit similar biophysical phenotypes in vitro. *Proc Natl Acad Sci U S A* **91**, 12785–12789.

Acknowledgements

The authors wish to thank the group 'Résocanaux' for fruitful discussions. We also thank F. Moueza, J.P. Bardon and M. Chastanet for their valuable technical help. This work was supported by the Institut National de la Recherche Scientifique (INSERM) and the Association Française contre les Myopathies (AFM).